Roles of Exposure Time and Geochemical Factors in the Characteristics of the Surface Sediments of the Hwangdo Tidal Flat, Taean, Cheonsu Bay, West Coast of Korea

Jun-ho Lee [1],*, Han Jun Woo [2], Hoi-soo Jung [3], Yeongjae Jang [4], Joo Bong Jeong [5], Keunyong Kim [6], Jae Hwan Seo [7] and Joo-hyung Ryu [8]

[1] Marine Domain & Security Research Department, Korea Institute of Ocean Science & Technology, Yeongdo-gu, Busan Metropolitan City, 49111, Republic of Korea

[2] Marine Domain & Security Research Department, Korea Institute of Ocean Science & Technology, Yeongdo-gu, Busan Metropolitan City, 49111, Republic of Korea; hjwoo@kiost.ac.kr

[3] Marine Domain & Security Research Department, Korea Institute of Ocean Science & Technology, Yeongdo-gu, Busan Metropolitan City, 49111, Republic of Korea; hsjung@kiost.ac.kr

[4] Korea Ocean Satellite Center, Korea Institute of Ocean Science & Technology, Yeongdo-gu, Busan Metropolitan City, 49111, Republic of Korea; yeongjae@kiost.ac.kr

[5] Marine Domain & Security Research Department, Korea Institute of Ocean Science & Technology, Yeongdo-gu, Busan Metropolitan City, 49111, Republic of Korea; jjbongeo@kiost.ac.kr

[6] Korea Ocean Satellite Center, Korea Institute of Ocean Science & Technology, Yeongdo-gu, Busan Metropolitan City, 49111, Republic of Korea; keunyong@kiost.ac.kr

[7] East Sea Environment Research Center, East Sea Research Institute, Korea Institute of Ocean Science & Technology, Uljin-gun, Gyeongsangbuk-do, 36315, Republic of Korea; playersjh@kiost.ac.kr

[8] Korea Ocean Satellite Center, Korea Institute of Ocean Science & Technology, Yeongdo-gu, Busan Metropolitan City, 49111, Republic of Korea; jhryu@kiost.ac.kr

* Correspondence: leejh@kiost.ac.kr

Abstract: The Hwangdo tidal flat is an intertidal landform located in Cheonsu Bay, Taean-gun, Chungcheongnam-do, on the west coast of Korea. The topographical characteristics of the semi-enclosed bay on the eastern side of the study area include waterways, sandbars, small islands, and tidal flats. In this study, data were acquired from tide gauges installed on the Hwangdo Bridge, and the height of the ellipsoid was measured using a real-time kinematics global positioning system (RTK-GPS). Digital elevation model (DEM) using Matrice 300 drone data were also acquired after processing. The geochemical sediment characteristics in the study area were analyzed, together with tidal-flat exposure-time characteristics based on environmental factors. Sediment data (n = 107) collected from October 25 to 28, 2022 (Korean local time) were used to classify sediment particles according to Folk and Ward (1957). Sedimentary facies ranged from coarse sand (sand:mud ratio = 9:1) to sandy silt (sZ) followed by muddy sand (mS) and slightly gravelly sandy mud ((g)sM). Total organic carbons (TOC) in the surface sediments were also characterized based on a particle-size analysis. The mean change in tidal height measured at Hwangdo Bridge during the sampling period was ~7.53 m (minimum: –3.86 m, maximum: +3.67 m). Based on the Boryeong's sea level measurement tide data in 2022, the tidal area in the drone images ranged from 6.362 m^2 (0.006 km^2) at DEM +4.0 to 4,841,078 m^2 (4.841 km^2) at DEM –4.0 m, indicating an increase in the annual tidal-flat area according to the tidal level of up to ~800-fold. The daily average exposure time was 9.0 h (minimum: 1.5 h, maximum: 17.9 h). Based on the results of multivariate analysis using exposure times and a geochemical dataset, four groups were identified: upper, middle, and lower intertidal zones and regions with a relatively high organic-matter concentration. A determination of the main characteristics of the Hwangdo tidal flat according to their spatial distribution showed that, among various environmental factors, changes in the sand or clay sediment composition were determined by community factors. This natural environmental condition did not affect the statistically significant relationship between tidal-flat exposure times and tide changes, which is a normal

topographical feature in the study area. The results of this study demonstrate the unique marine environmental characteristics in the Hwangdo tidal flats.

Keywords: exposure time; geochemical factors; Hwangdo Tidal Flat

1. Introduction

Coastal bays are broadly divided into estuary bays and semi-enclosed bays. An estuary bay connects an estuary with the open sea and is thus exposed to circulation of ocean currents and to freshwater inputs from river flows. A semi-enclosed bay receives little inflow of freshwater from land and the circulation of seawater to and from the open sea is limited by one or several restricted channels. Accordingly, seawater circulation, sedimentation processes, and ecosystem and sediment characteristics will differ depending on the type of bay [1].

The west coast of the Korean Peninsula is an area of shallow water and a wide continental shelf. Its estuaries, bays, and tidal flats were formed by sea-level rise after the Pleistocene. This led to the formation of a ria coast that accounts for the various types of coastal environments, although meteorological events, such as storms and typhoons, have also determined the coastal features [2,3]. The large tidal flat consists of sediments that vary in their type and their characteristics [4].

In the 1960s, a period that initiated the rapid growth of developing countries, including South Korea, large areas of the tidal flats were lost due to coastal development, including agriculture, industry, new town construction, and large-scale land reclamation projects. These environmental changes caused hydraulic changes in the tidal flats, adversely affecting their sedimentary environments and ecosystems, such as by the erosion/deposition of coastal sediments due to increased coastal pollution resulting from inflow of pollutants from land and changes in ocean currents and tides due to changes in the coastline [1].

The geographical features of the study area include the estuaries of the Han River and the Geum River, and the interior of bays, which together with coastal development determine depositional mechanisms [1]. The unique characteristics of the west coast of Korea have been examined in sedimentological studies [5–8], including those of surface sediments [1,9,10], and long-term changes in the sediments and topography of the western and southern coasts [8,11,12]. These studies have shown regional hydraulic changes that affect the marine environment, including the sedimentary environments of the tidal flats and therefore their biodiversity as well as their ability to supply nutrients to nearby waters and to remove pollutants [13].

Cheonsu Bay is located on the central coast of the West Sea. The Hwangdo tidal flat is an intertidal landform located in Cheonsu Bay, Taean-gun, Chungcheongnam-do, on the west coast of Korea. Seawater enters the bay and the waterway under the Anmyeon-do suspension (land) bridge. Prior to the 1980s, the bay was free of contaminants, as there was no inflow of large rivers, and biological productivity was high, making it suitable for aquaculture. However, the construction of seawalls near the study area from 1983 to 1985 resulted in the creation of Lake Ganwol and Lake Bunam, which caused significant changes in the sedimentary environment and ecosystem of Cheonsu Bay. In the 1998's found that, after construction of the embankment, the absolute flow velocity in the northern part of the bay decreased greatly, and the exposure time of the northern tidal flat increased [14].

The marine environment before and after construction of the embankment in Cheonsu Bay has been extensively investigated [14–17]. In the 1979's examined the sedimentation and sedimentary environment of Cheonsu Bay before construction of the embankment [18]. And other researchers have focused on the post-construction characteristics and the distribution of the tidal flats, sediments, and waterways [19–22]. The surface sediments consisted of five sedimentary facies, as determined in June and October 2003, and sediment accumulation rates in the Hwangdo tidal flat over a period of 11 months indicated sediment deposition in the central part, whereas the eastern and western sides of the tidal flat had eroded [1]. An analysis of high-spatial-resolution remotely sensed data (IKONOS

and KOMPSAT-2, Korea multi-purpose satellite-2) showed that the percentage of grains larger than very fine sand (0.0625 mm) at the Hwangdo tidal flat had increased considerably since the early 2000s. Mud-flat facies decreased by 5.81% in the late vs. the early 2000s, whereas mixed mud flats and sand flats increased by 4.46% and 2.14%, respectively [23].

This study examined recent dynamic changes in the tidal flats in north Cheonsu Bay. Specifically, geochemical sediment characteristics (n = 107) measured in 2022 in the Hwangdo tidal flat were analyzed to determine the interaction of tidal-flat exposure with various environmental factors, and their correlation.

2. Materials and Methods

The Hwangdo tidal flat of Cheonsu Bay, Taean-gun, Chungcheongnam-do is located on the central coast of the West Sea and is characterized by a diverse and complex environment and topography [1]. Seawater enters the bay and the waterway under the Anmyeon-do suspension (land) bridge. Cheonsu Bay surrounds Anmyeondo Island in Taean County, Ganwoldo Island in Seosan City, and West Sea line in Boryeong City, as shown in Figure 1 (a) and (b). The total surface area was originally 380 km^2, but it was reduced to ~180 km^2 following the construction of an embankment as part of the Seosan A and B District reclamation project in 1984, the creation of Buam Lake and Ganwol Lake, and the construction of a second embankment as part of the Hongbo District reclamation project [14]. The Cheonsu Bay is semidiurnal tide, with a maximum high tide of 633 cm, a minimum low tide of 286 cm, and an average tide of 459 cm. The 1.65-km wide × 5.15-km long Hwangdo tidal flat is adjacent to Anmyeon Island in Cheonsu Bay and it includes complex tidal channels. The sedimentary facies in the study area are composed of facies deriving from high tide and low tide, mixed facies, and sand facies [24]. The sampling stations for the surface sediments (n = 107) are shown in Figure 1 (c) and (d).

The Hwangdo tidal flat is gentle and broad with an average slope of < 0.1 cm and a highly varied topographical structure that includes tidal channels ranging in width from 2 cm to 200 cm, chenier, and sand shoals. These topographic features affect the tidal flow and thereby the sediment-distribution characteristics and the topographical elevations. The latter affect the optical reflectivity by altering the exposure time depending on the state of the tide [23]. In this study, the terrain altitude of the Hwangdo tidal flat was examined using Leica's Real Time Kinetic-Global Positioning System (RTK-GPS).
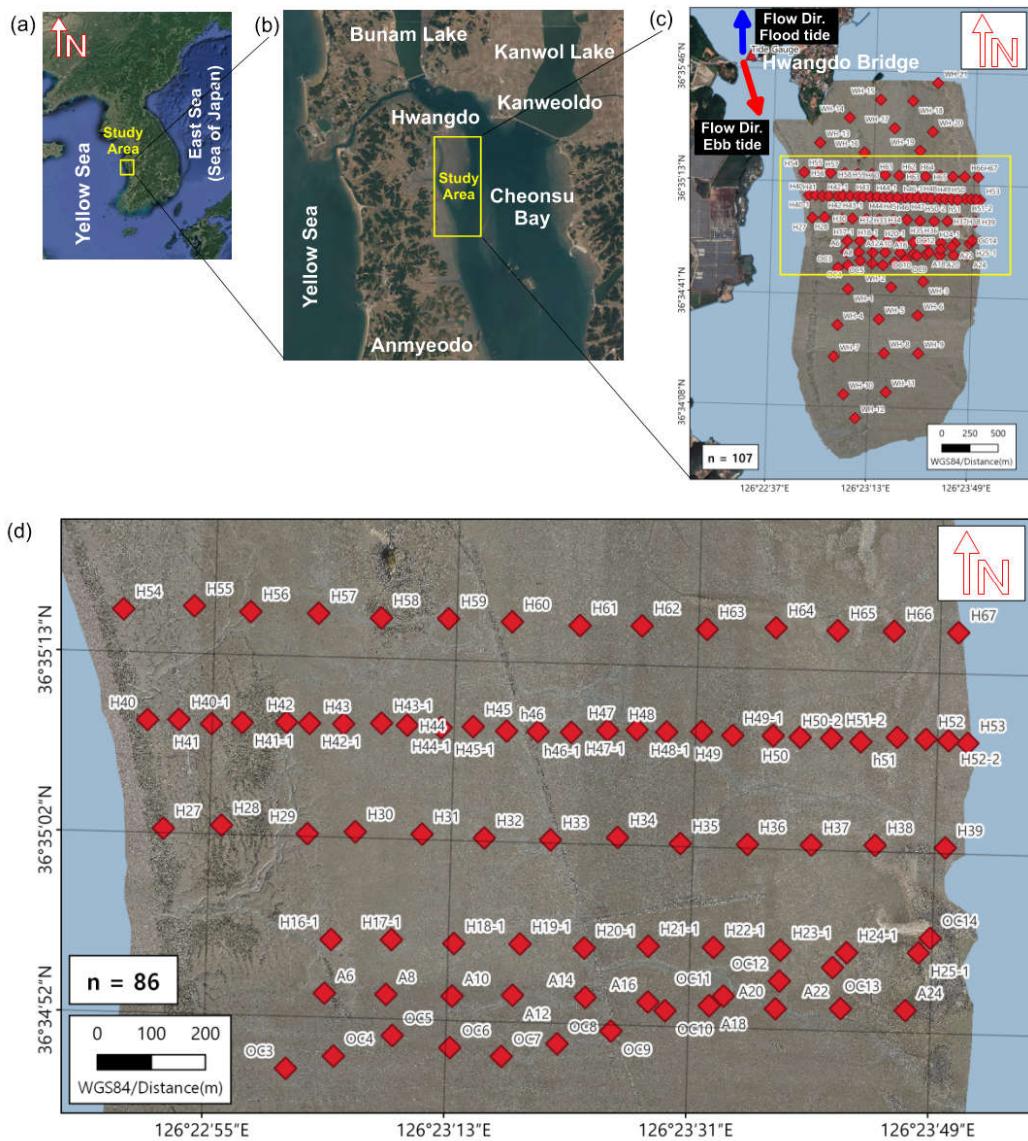
Figure 1. Map of the study area. (a) Location of the study area within South Korea. (b) Detailed map of the study area, showing Hwangdo tidal flats, Taean, Cheonsu Bay, west coast of Korea. (c) Red rhombi indicate the surface-sediment sampling stations (n = 107). (d) Enlarged map of the sampling stations (n = 86).

A drone survey was conducted using a full-frame sensor (Matrice 300 drone RTK-GPS + GLONASS + BeiDou + Galileo; DJI) as shown in Figure 2 (a) and (b). Orthophotos were taken along the route and ground photos were taken from ground-control-point (GCP) stations (n = 17) using the Matrice 300 drone. In addition, tide gauges were installed at Hwangdo Bridge in Figure 2 (c). The 3D error of each vertex was set to be within 0.02 m. RTK-GPS was operated using both a reference station and a mobile station. At the former, the reference point was set using the coordinates of the integrated reference point provided by the National Geographic Information Institute, South Korea. A moving RTK was obtained using a pole with a length of 2 m that supported a flat object in the center of the apex surface layer, with the end of the pole fixed to the flat object to measure the orthometric height (Figure 2 (b)). The mean change in tidal height measured at Hwangdo Bridge during the sampling period was ~7.53 m (minimum: –3.86 m, maximum: +3.67 m).
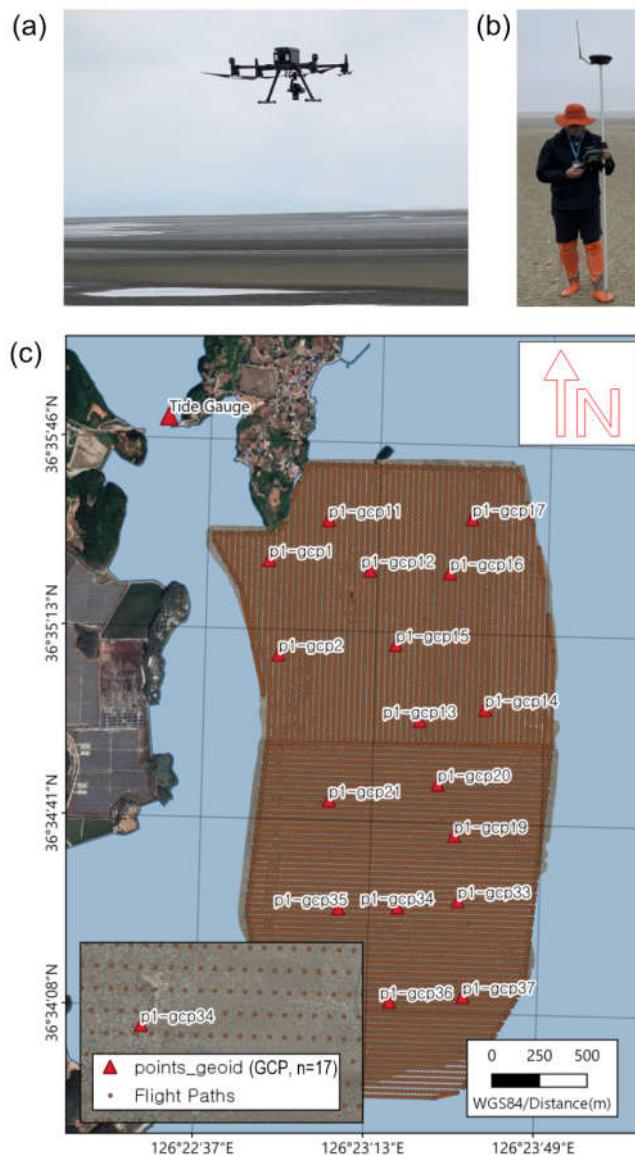
Figure 2. Field survey using drones for digital elevation model (DEM) processing. (a) Drone survey using a full-frame sensor (Matrice 300 drone Real-Time Kinematic-Global Positioning System (RTK-GPS) + GLONASS + BeiDou + Galileo; DJI). (b) RTK-GPS station for measuring tidal-flat elevations using a rover. (c) Orthophoto taken route and at a ground control point (GCP) station (n = 17) using a Matrice 300 drone. The location of Hwangdo Bridge, where the tide gauges were installed during the survey period, is also shown.

Samples (~1 kg) were collected from the sediment surface (at depths of up to 1.0 cm) using a clean spoon and stored in the dark in an icebox (< 4°C) until delivery to the laboratory. The actual tidal change at Hwangdo Bridge from October 25 to October 28, 2022 is shown in Figure 3 (a), (c), and (d). Hwangdo Bridge was constructed in December 2011 by removing the embankment connecting Anmyeon-do and Hwang-do, Taean-gun in Figure 3 (b). After the opening of the bridge, the seawater distribution resulting from the bridge construction improved the marine environment, including an increase in the productivity of the nearby tidal flats [25].
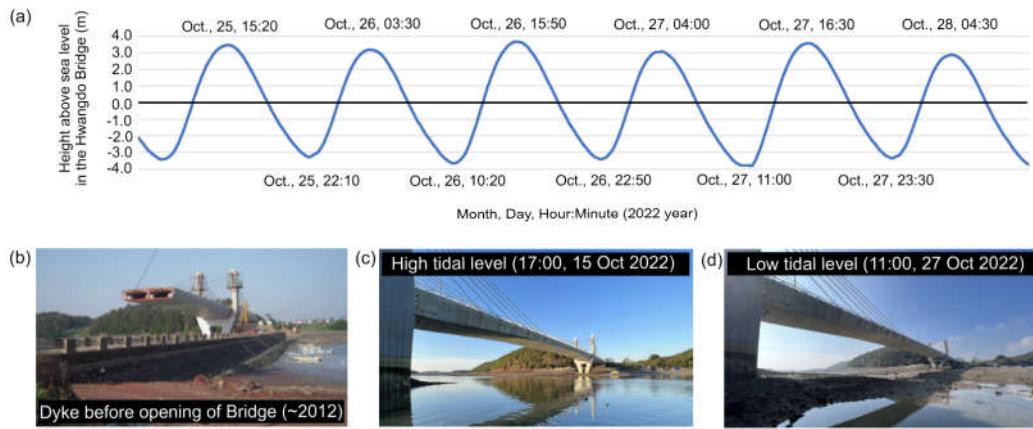
Figure 3. Hwangdo Bridge, the site of the installed tide gauges, and graphs of the tide-level changes during the survey period. (a) Actual tidal change at Hwangdo Bridge from October 25 to October 28, 2022. (b) The seawall constructed in 2012, before the construction of Hwangdo Bridge [25]. (c) High tide on October 15, 2022. (d) Low tide on October 27, 2022.

The grain-size distribution of sediment particles was analyzed following a standard sieving procedure [26] to obtain the sand fraction (particle size < 4 Φ). The mud fraction (> 4 Φ) was obtained by examining samples at 0.5-Φ intervals using a particle-size analyzer (SediGraph 5100; Micromeritics, Norcross, GA, USA) at the Korea Institute of Ocean Science and Technology (KIOST). An inclusive graphic method was used to determine sediment type, mean size (Φ), sorting (Φ), and skewness and kurtosis [27].

For total organic carbon (TOC) and total nitrogen (TN) analyses, 10 mL of 1 N HCl was added to 0.5 g of powdered sediment overnight to remove carbonate materials. The samples were then re-dried and re-weighed, with the difference recorded as the TOC. Both TOC and TN were measured using an elemental analyzer (FlashEA 1112; Thermo Fisher Scientific, Waltham, MA, USA) at KIOST, by placing a few milligrams of treated sediments in an aluminum capsule. To ensure the reliability of the analytical data, two soil reference materials from the National Institute of Standards and Technology of the United States (nos. 338-40025 and 338-35210, Thermo Fisher Scientific) were included in the analysis. The total inorganic carbon (TIC) content was calculated as total carbon (TC) (%) – TOC (%), and the total calcium carbonate content, based on the relative percent difference (%), as shown in Equation (1) [28,29].

$$CaCO_3(\%, TIC) = (TC - TOC) \times 8.33$$

$$RPD = \frac{[(Carbon_{sample\ 1} - Carbon_{sample\ 2})]}{[\frac{(Carbon_{sample\ 1} + Carbon_{sample\ 2})}{2}]} \times 100 \tag{1}$$

To determine porewater salinity, a sediment sample of ~50 g was placed in a 50-mL Falcon tube and centrifuged at 2500 rpm for 10 min. The supernatant was then used to measure the electrical conductivity.

Since the sediments of tidal flats are always in contact with seawater, a sediment analysis must also consider the seawater in the pores between particles (interstitial water content, IWC) and the seawater on the surface of the tidal flat (surface water cover, SWC) [30]. The nature of the seawater present in tidal flats will vary depending on the sediment particle size, the topography (slope) of the tidal flat, the exposure time, *etc.*, and will affect the optical reflectivity [31]. In this study, SWC was not measured, while IWC was measured as the difference between the weights of the sediment before and after drying at 100°C. The moisture content was measured based on the weight change. Dry bulk density (g/cm³) was defined as the ratio of the weight of the dry sample (W_d) and the total sample volume (V_t) and represents the mass of dry solids in a given bulk volume (5 ml) of sediment [32,33].

Another important characteristic of sediments is their porosity (ϱ), defined as the percentage of the total volume not occupied by solid particles, as shown in Eq. (2). In flooded sediments, this is equivalent to the volumetric percentage of water in the sediment [33].

$$\rho = 100 \times (V_w/V_t) = 100 \times (V_t - V_s)/V_t \qquad (2)$$

where V_w is the volume of water, V_t is the total volume of a sediment sample, and V_s is the sum of the volume of the solids.

The porosity (ϱ) of the sediment can be also calculated based on the relationship between its dry bulk density and the particle density [34], as shown in Eq. (3):

$$\rho = \left(1 - \frac{\text{bulk density}}{\text{particle density}}\right) \times 100 \qquad (3)$$

On October 26, 2022, a drone survey was conducted. The DEM was completed using the actual tidal data determined at Hwangdo Bridge, the drone data, and the GCP during the study period. The exposure time was calculated according to the tide-level change. The quality of the final processed data of the DEM was 1 m^2 per DEM pixel. Data from 2022 were obtained by correcting the tidal-gauge data according to Korea Hydrographic and Oceanographic Agency (KHOA) in the Boryeong's sea level measurement tide area.

In the multivariate analysis (MVAs), environmental variables were square-root-transformed and a cluster analysis and a non-metric multidimensional scaling (MDS) analysis were performed using an Euclidean distance matrix [35]. A MVAs is based on the multivariate statistics and is used to address situations in which multiple measurements of each experimental unit are made and the relationships among those measurements and their structures are important. MVAs include normal and general multivariate models and distribution theory, the study and measurement of relationships, probability computations of multidimensional regions, and exploration of data structures and patterns. In this study, a principal coordinate analysis (PCA) was applied to determine the major abiotic parameters influencing the spatial distribution. MVAs were performed using Primer 7 + PERMANOVA statistical software (Plymouth Marine Laboratory, Plymouth, UK).

3. Results

In total, 13 surface facies were distributed throughout the study area. The sedimentary facies were classified following Folk and Ward [27]. Based on 107 sample groups, four facies types were identified. Group 1 (n = 10) consisted of slightly gravelly sand ((g)S), gravelly sand (gS), and sand (S); group 2 (n = 73) consisted of slightly gravelly muddy sand ((g)mS), gravelly muddy sand (gmS), muddy sand (mS), muddy sandy gravel (msG), and silty sand (zS); group 3 (n = 20) consisted of slightly gravelly sandy mud ((g)sM), sandy mud (sM), and sandy silt (sZ); and group 4 (n = 4) consisted of gravelly mud (gM) and mud (M). The sedimentary facies ranged from coarse sand (sand : mud ratio = 9:1) to sandy mud, in proportions of sandy silt (sZ) > muddy sand (mS) > slightly gravelly sandy mud ((g)sM). The respective mean values (range:) of gravel, sand, silt, and clay were 1.15% (0.00%–30.70%), 59.87% (6.98%–96.64%), 25.11% (0.15%–55.84%), and 13.86% (0.30%– 39.42%). The average sediment grain size was +4.35 Φ (−0.31 to +7.33 Φ). The average sorting was +2.27 Φ (+0.61 to +4.52 Φ), indicative of moderately well sorted to extremely poorly sorted sediment grains. The average skewness and kurtosis was +0.55 (–0.26 to +0.76), with a positive value (tail to the right) when the proportion of coarse sediment was large. The centrally concentrated and mostly centrally concentrated leptokurtic values had a mean of +1.90 (range: +0.51 to +5.59) and thus moderately good to extreme characteristics in terms of their mean sorting degree. The distribution of surface sediments was generally fine-grained sandy mud sediments in the west, muddy sand sediments in the central region, and coarse gravelly sand sediments in the east.

The average TOC, TC, TN, and TIC contents were 0.17% (range: 0.02–0.61%), 0.30% (0.13–1.16%), 0.02% (0.00–0.08%), and 1.06% (0.01–6.66%), respectively. The overall density was 1.34 g/mL (0.91–1.53 g/mL), the average porosity was 0.44% (0.18–0.63%), and the average water content was 25.87% (8.89–42.69%). The density tended to decrease as the average particle size decreased, whereas the

moisture content and porosity showed the opposite trend. The TOC/TN ratio was consistently ≤ 10, which implies the influence of marine rather than terrestrial organisms. The average porewater salinity was 39.52 psu (range:11.00–57.13 psu). The organic matter was characterized based on an analysis of particle size and the results confirmed the experimental values.

The average elevation values based on data from the 107 stations ranged from –0.66 m (–2.71 to +1.70) as shown in Figure 4. The relationships between the sedimentary environmental factors and the topography of the intertidal zone were investigated using the Hwangdo tidal-flat intertidal DEM created by the GCP-drone orthogonal remote sensing method. Although this method is far less accurate than a leveling of sight lines, it is effective in assessing the overall topography of an intertidal zone [36]. The topographical distribution was similar to that indicated by the orthometric height, with slopes rising slightly to the west (Figure 4). The overall trend showed a topography with a high center, with peaks slightly skewed to the west and steep slopes in the west, while the eastern slope was relatively gentle. The two sandbars located to the east had very high altitudes. In the western area, of around 0 m altitude, the features of the drone image were those of highly developed tidal channels. The overall trend showed a topography with a flat center, slightly tilted to the west, a gentle slope to the east and a sharp slope towards the western side. The two sandbars located in the east were of very high altitude. In the area ~2 m above sea level, the tidal channels and valleys were well-developed according to the DEM data, while the altitude of the rest of the area was relatively low. In terms of particle-size composition, pearl (pearl component 36.7–95.2%) was predominant in the western region in the north-south direction, corresponding to the ridge of the upper intertidal zone of the Hwangdo tidal flat, and sand in the two sandbar sedimentary facies in the east (sand component 75.7–96.6%). This distribution reflects the development status of the main and minor channels, the presence or absence of surface residual water, and the topography [37–39].
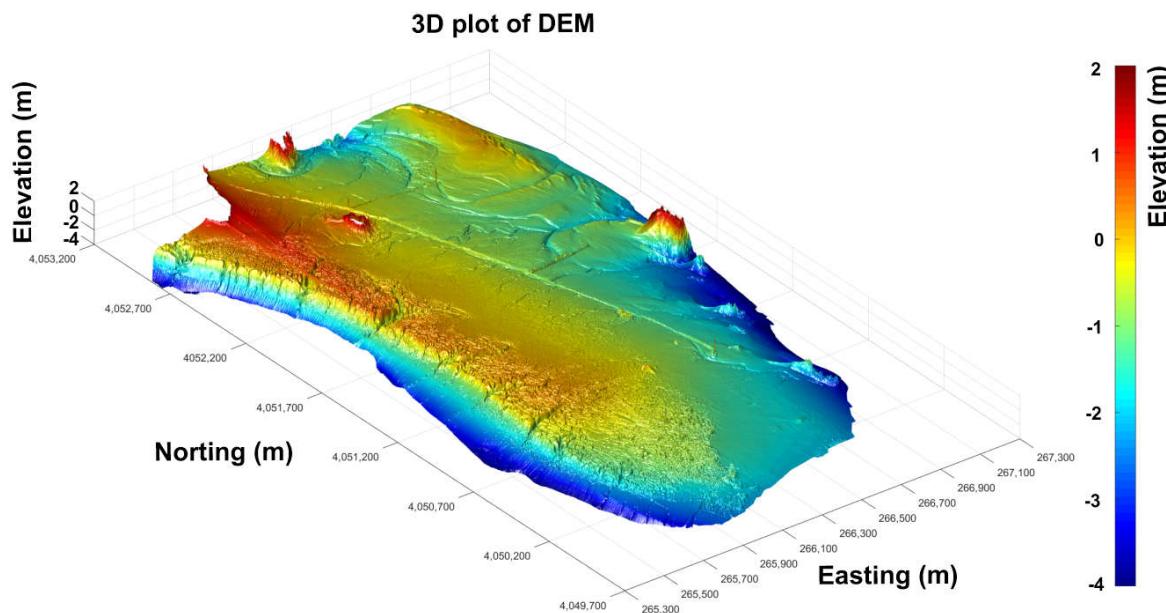
Figure 4. 3D plot after DEM processing using the orthophoto taken route using a Matrice 300 drone.

The above results show that the distribution of the tidal currents in the west of the Hwangdo tidal flat is closely related to topographical features. For reference, high-resolution images (IKONOS RGB (432 bands)) together with the DEM can be used to classify three types of sedimentary facies: mud, mixed, and sand sedimentary, considering the sedimentological characteristics of the intertidal zone, including the surface-layer size, surface residual water, tidal-channel distribution, and topography [40].

Analysis of DEM profile lines showed that the changes in the elevation values of each of the eight latitudes decreased gradually as latitude decreased (H1 to H8 lines), and the overall topography

distribution ranged from high to low in Figure 5 (a) and Figure 6 (a). The central region did not show a relatively large change according to latitude change. However, as expected, the two sandbars located in the east had relatively high altitudes. The 4.3-m elevation easting to 478 m on the H1 line was the topographical portion of the land portion. At the H4 line easting at 1,832 m, the elevation of 1.4 m represented a relatively high rock formation at the sandbar. The DEM-profile-line analysis showed that the elevation decreased rapidly with decreasing latitude. In addition, the elevation in the north increased irregularly from west to east, whereas the elevation in the south decreased, as shown in Figure 5 (b) and Figure 6 (b).
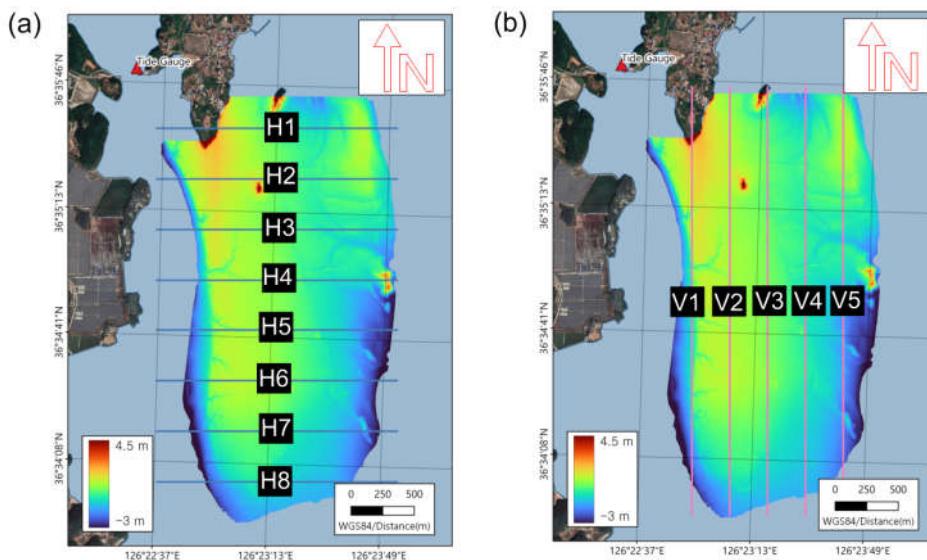
Figure 5. Line selection for elevation analysis. (a) Lines used in the analysis of elevation changes by latitude using DEM data. (b) Lines used in the analysis of elevation changes by longitude using DEM data.
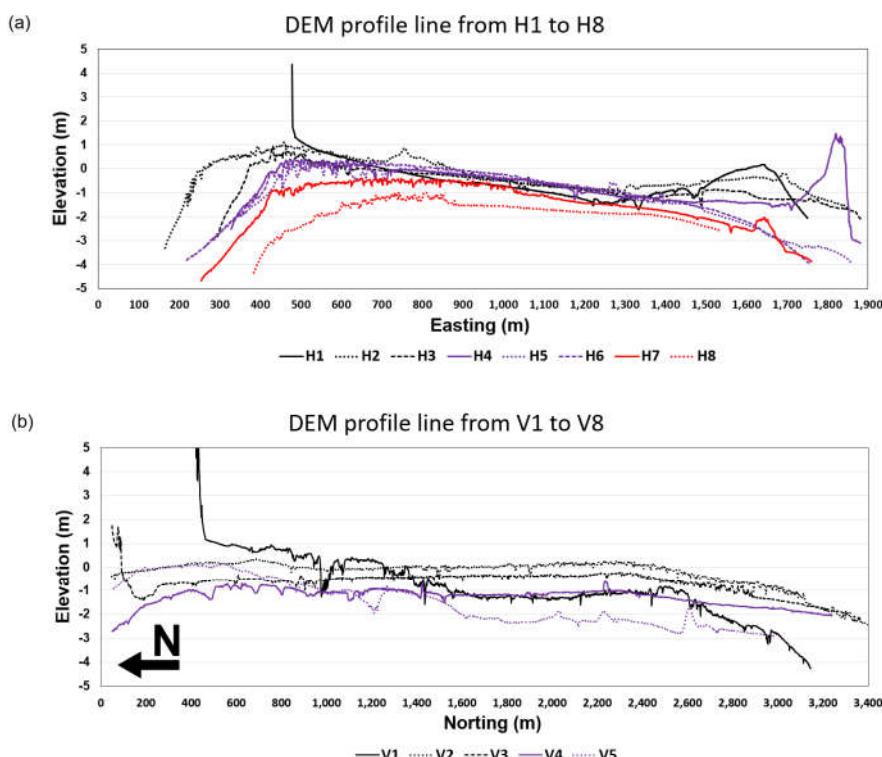
Figure 6. Elevation changes by longitude and latitude. (a) Altitude changes by latitude from H1 to H8. (b) Altitude changes by longitude from V1 to V5.

The area-change value according to the tidal-level change of the tidal flat was examined as well. The area at -4.0 m elevation was the maximum area range captured by the drone. At –4.0-m elevation, the exposed area was 4.841 km². With an increasing tidal level, only the high-elevation topography of the western part of the Hwangdo tidal flat remained at the 0.0 m mark, corresponding to an area of 0.800 km². The area with the largest increase in the rate of exposed area (Δ) at a tidal interval of 1 m or 0.5 m occurred at an elevation change from +2.0 m to 1.0 m, with an increase in the exposure area of 323%. Thereafter, the rate of increase gradually decreased as the altitude decreased. The tidal-flat exposure time is shown in Figure 7 (a)-(l) and Table 1 (25–28 Oct. 2022). The highest exposure-time ratio in the study area was within ~12 h, with an area of 2.47 km², and a rate of 50.8% on 26 Oct. Similarly, according to the 2022 KHOA, the highest exposure-time rate was within ~12 h, with an area of 2.48 km² and a rate of 51.1%. A calculation using the actual measurement data from the Boryeong's sea level measurement tide data for the year 2022 showed that the highest exposure-time rate was within ~12 h, with an area of 1.43 km² and a rate of 29.5%. The drastic reduction during the period 25 to 28 Oct. 2022 compared to the control period can be explained by the tide level, in which the greatest changes occurred twice a month on average throughout the year, when corrected by the Boryeong tide gauge for 2022 in Figure 8 (a)-(c) and Table 2.
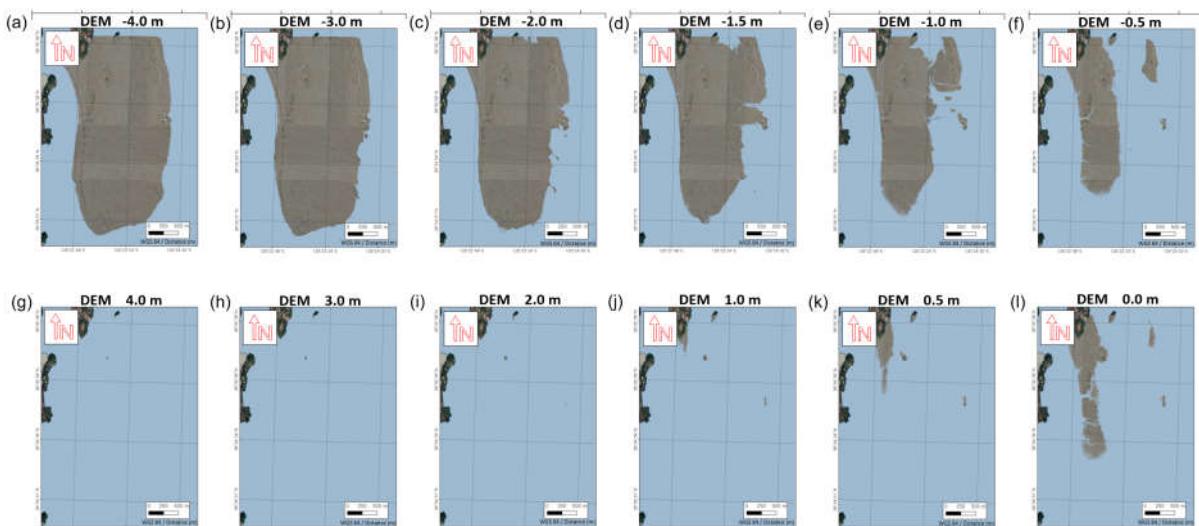
Figure 7. Changes in the exposed area of the tidal flats in the study area based on changes in the tide level (DEM –4.0 to 4.0 m).
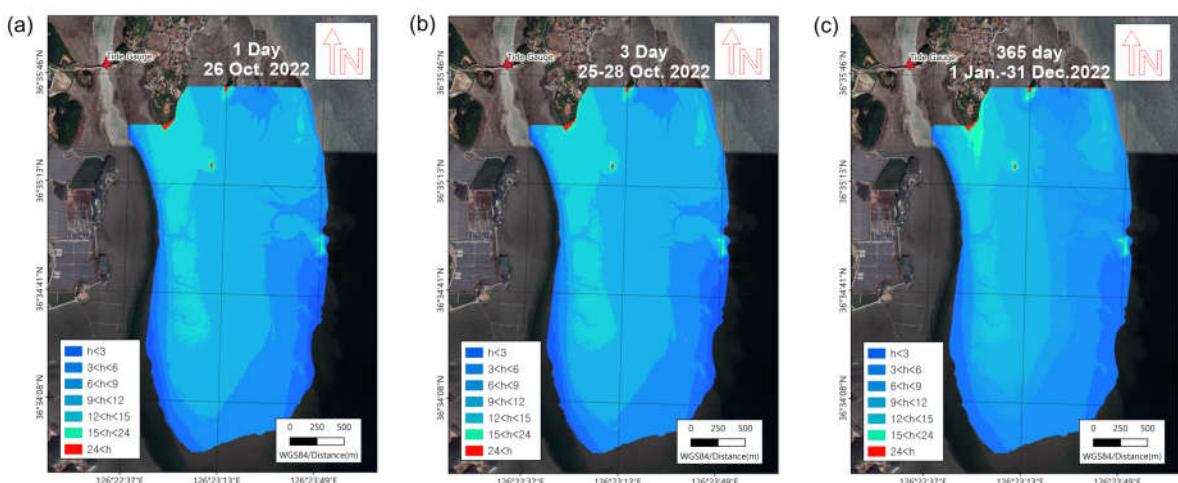
Figure 8. Comparison of exposure times in 2022 according to the research period processing method. Exposure-time images obtained (a) on October 26, 2022, (b) between October 25 to 28, 2022, and (c) for the year 2022 according to Korea Hydrographic and Oceanographic Agency (KHOA).

Table 1. Changes in the exposed areas (m², km², and Δ%) of the tidal-flat in the study area based on changes in the tide level (DEM –4.0 to 4.0 m).

Tidal level (m)	Exposed area (m²)	Exposed area (km²)	Exposed area (Δ, %)	Tidal level (m)	Exposed area (m²)	Exposed area (km²)	Exposed area (Δ, %)
+ 4.0	6,362	0.006	-	-0.5	1,728,087	1.728	116
+ 3.0	8,274	0.008	30	-1.0	2,740,140	2.740	59
+ 2.0	13,494	0.013	63	-1.5	3,561,450	3.561	30
+ 1.0	57,126	0.057	323	-2,0	4,149,875	4.150	17
+ 0.5	215,435	0.215	277	-3.0	4,640,762	4.641	12
0.0	799,813	0.800	271	-4.0	4,841,078	4.841	4

Table 2. Comparison of exposure times in 2022 according to the research period processing method (1 day, 3 days, and the year 2022 according to Korea Hydrographic and Oceanographic Agency (KHOA)).

Exposure time (h) (Guideline: 1 Jau. 2022-31 Dec. 2022, 1year)	Exposed area (m², km²)	Exposed area (%)	Exposure time (h) (Guideline: 25-28 Oct. 2022, 3 day)	Exposed area (m², km²)	Exposed area (%)	Exposure time (h) (Guideline: 26 Oct. 2022, 1 day)	Exposed area (m², km²)	Exposed area (%)
≤ 3 h	557,753 0.56	11.5	≤ 3 h	168,772 0.17	3.5	≤ 3 h	151,850 0.15	3.1
~ 6 h	1,251,492 1.25	25.7	~ 6 h	289,550 0.29	6.0	~ 6 h	347,895 0.35	7.2
~ 9 h	1,048,798 1.05	21.6	~ 9 h	1,153,271 1.15	23.7	~ 9 h	1,226,007 1.23	25.2
~ 12 h	1,433,997 1.43	29.5	~ 12 h	2,467,386 2.47	50.8	~ 12 h	2,484,270 2.48	51.1
~ 15 h	500,274 0.50	10.3	~ 15 h	755,080 0.76	15.5	~ 15 h	628,871 0.63	12.9
~ 18 h	52,503 0.05	1.1	~ 18 h	16,386 0.02	0.3	~ 18 h	12,224 0.01	0.3
~ 21 h	6300 0.01	0.1	~ 21 h	2632 0.00	0.1	~ 21 h	2168 0.00	0.0
~ 24 hour	4025 0.00	0.1	~ 24 hour	1371 0.00	0.0	~ 24 hour	1137 0.00	0.0
~ 24 hour < (at all times)	6175 0.01	0.1	~ 24 hour < (at all times)	6869 0.01	0.1	~ 24 hour < (at all times)	,895 0.01	0.1
Sum	4,861,317	100	Sum	4,861,317	100	Sum	4,861,317	100

4. Discussion

The spatial distribution of the Hwangdo tidal-flat stations was primarily determined by variations in sediment composition. Based on the cluster analysis and MDS the stations located at the tidal flat were divided into four groups (A, B, C, and D), representing upper, central, and lower stations, and regions of high organic-matter concentration, respectively (Figures 9 and 10). In the dimension one (D1) in Figure 10, the distance of two points present on the real line is the absolute value of the arithmetic difference of the coordinates (D1(p, q) = |p−q|). The major environmental variable in group A (upper stations) was the sand composition; in group B (central stations), it was the mean particle size and silt; in group C (lower stations) it was the sand composition; and in group D it was the high organic carbon concentrations.
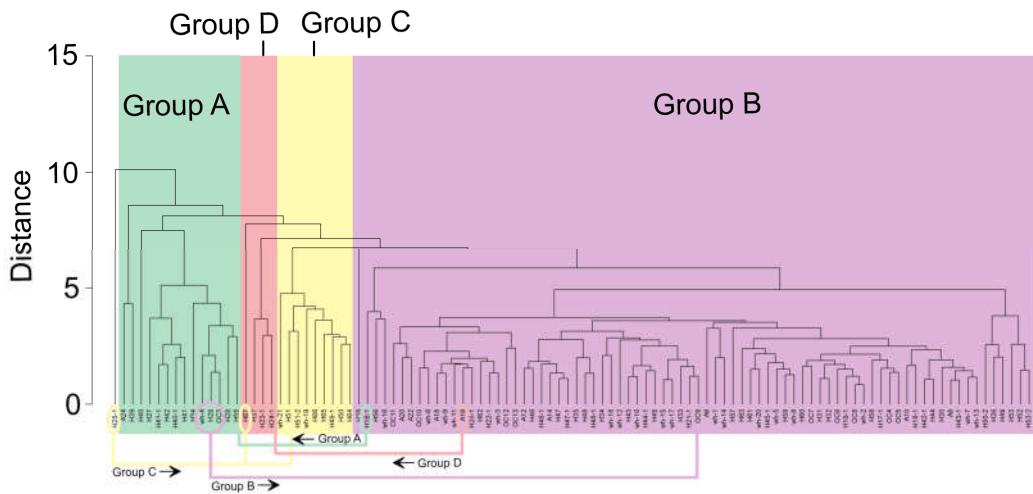
Figure 9. Cluster analysis of the square-root-transformed environmental variables.
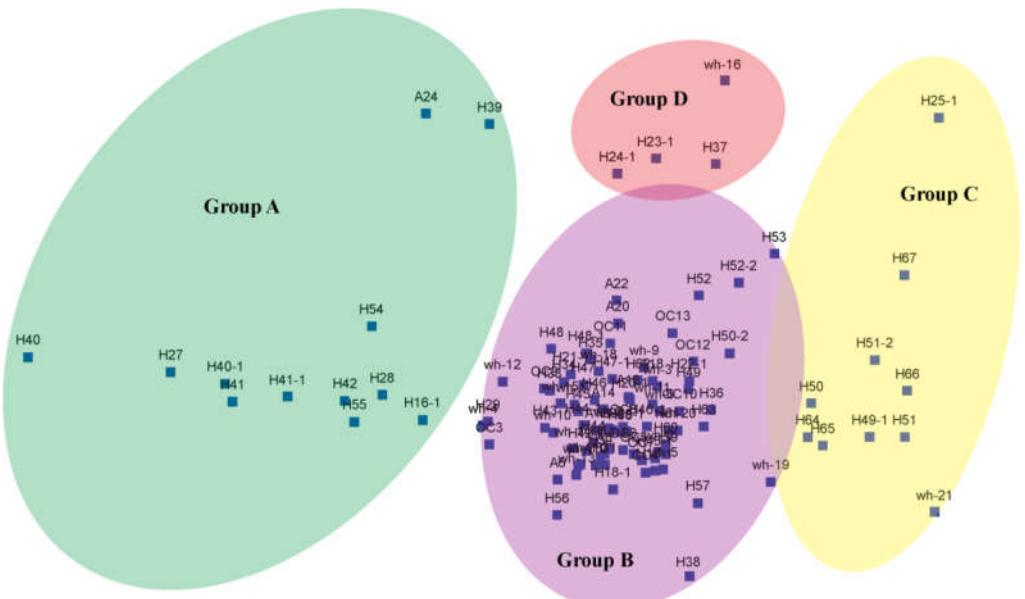
Figure 10. Multidimensional scaling **(**MDS) based on the D1 Euclidean distance using the square-root-transformed data.

The degree to which the combinations of the various factors affected the formation of the tidal-flat groups in the ecliptic plane was determined. The closer the value to 1, the stronger the correlation (Table 3). Among the analyzed factors, the single most influential was the average particle size. Combining the factors increased their degree of influence on group formation, but the differences were small and complicated explanations of the effect of each factor. The main factors influencing the formation of the Yellow Island tidal-flat group were sand, silt, and clay contents, which also collectively determined the average particle size.

Table 3. Best result for each combination of variables among the environmental factors, based on Spearman rank.

Rank	Factor and value
1	Mean size (Mz)
	0.780

2	Mean size (Mz), Sorting
	0.855
3	Mean size (Mz), Sorting, TIC
	0.888
4	Mean size (Mz), Sorting, TIC, Skewness
	0.889
5	Mean size (Mz), Sorting, TIC, Skewness, Dry bulk density
	0.891

The correlation between the exposure time and the spatial distribution of the sediment composition was low (Figure 11). The tides near the tidal channel to the west of Hwangdo are of relatively low energy, which affects the tidal flats, with increasing sedimentation in the central area. At Cheonsu Bay, man-made structures such as seawalls have altered seawater circulation. The resulting changes in sedimentation patterns and flow have contributed to changes in the current and thus in the sedimentary phase of the surface sediments of Hwangdo. Figure 12 and Table 4 shows the grouping by upper, middle, lower intertidal zones and the area of high organic-matter content.
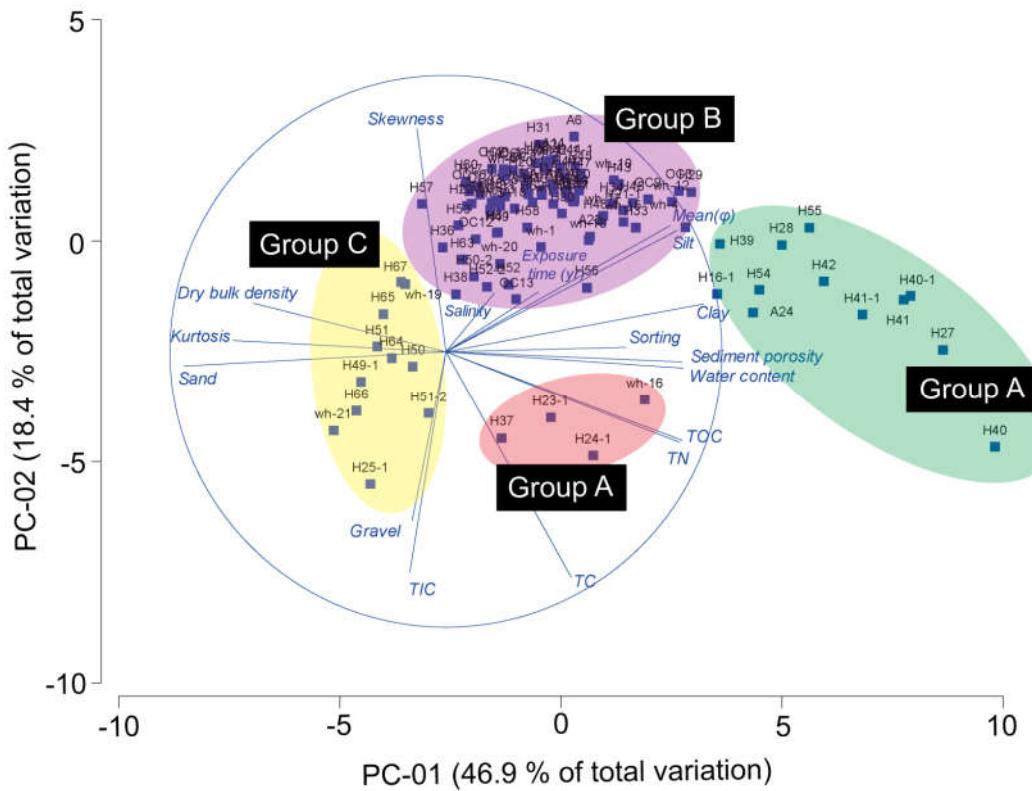
Figure 11. Principal components analysis (PCAs) of environmental variables.
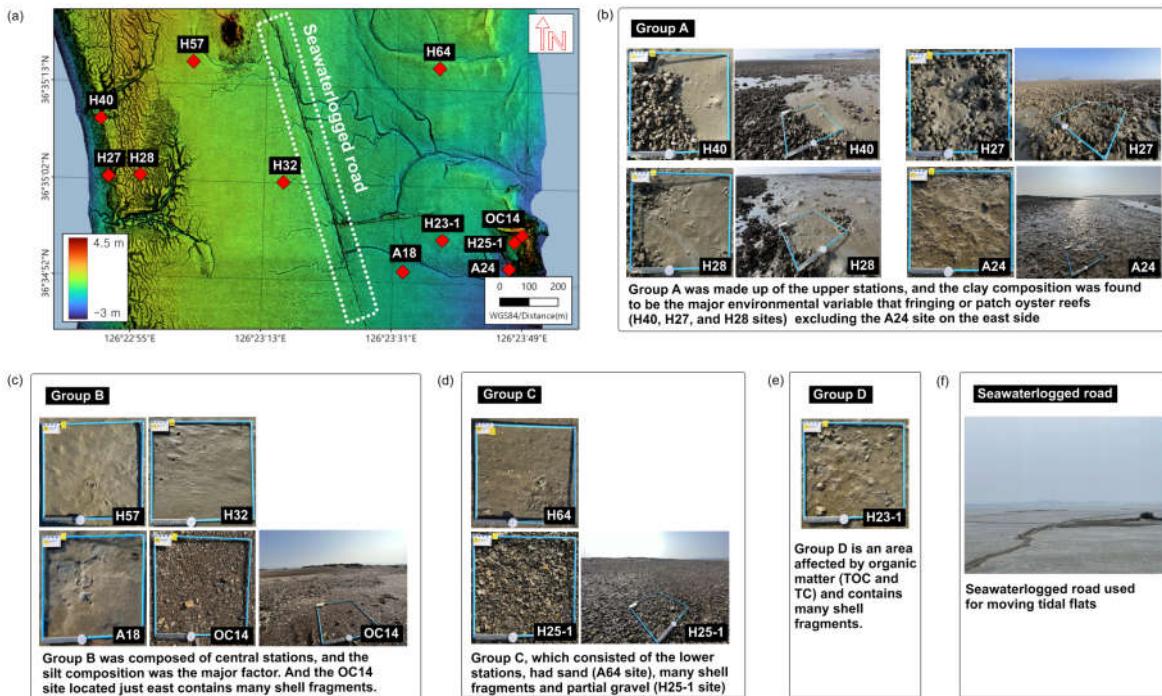
Figure 12. Grouping by upper, middle, and lower intertidal zone and the area of high organic matter. (a) Map of the station sites. (b) Orthogonal scale bar (50 × 50 cm) and landscape photos of the area in group A (c), group B, (d) group C, and (e) group D. (f) The Seawater-logged road used to access the tidal flats.

An analysis of the oyster-reef area showed an increase in 2019 compared to 2015, based on the linear spectral unmixing classifications obtained with the KOMPSAT-2/3 data [41]. By contrast at the H40, H27, and H28 stations, high tidal-channel-index values indicative of a dendritic pattern of tidal-channel distribution were identified in areas of high elevation and fine-grained sediments, as determined using remotely sensed data such as those from the KOMPSAT-2, Landsat Enhanced Thematic Mapper Plus (ETM+), and aerial photographs [42]. A previous study [43] confirmed our choice of a statistical approach to intertidal classification and topography to monitor the near-real-time spatiotemporal distribution changes in the tidal flats using continuous and stable Synthetic Aperture Radar (SAR) data obtained at local and regional scales. The dataset generated in this study can be used for field verification.

In October 2022, data on sedimentary-environment factors, such as geochemical data and topographical-elevation data, were obtained using drones, and data on the surface sedimentary facies vertex were obtained by analyzing the surface sediments. Thirteen types of sedimentary facies were identified. The distribution of surface sediments was generally fine-grained sandy mud sediments in the west, muddy sand sediments in the central region, and coarse gravelly sand sediments in the east. In the study by Kim *et al.* [44], data on sedimentary environmental factors, such as surface sedimentary facies and elevation between 2004 and 2013, were obtained in field surveys, and the soil moisture content of each sediment was measured to analyze the correlation between seawater and optical reflectance in the tidal flat. The results showed 12 sedimentary facies distributed in the Hwangdo tidal flat, with a gradual increase in the sand content and elevation between 2004 and 2013.

In a previous study [40], the classification of sedimentary facies using IKONOS RGB (432 bands) images collected over the Hwangdo tidal flat in Cheonsu Bay was qualitatively investigated. The optical reflectance was compared with environmental and sedimentary factors such as grain size, tidal-channel patterns, and the presence of surface remnant water. The results showed that satellite images of high spatial resolution, such as those from IKONOS, can be used to classify surface sedimentary facies (mud, mixed and sand) if tidal sedimentary characteristics, including grain size, surface remnant water, and the tidal channel network, are considered as well.

Table 4. Summary of sedimentary environments at re-presentive sampling sites.

Group	Station No.	Sedimentary type and Facies (Folk 1957)	Sand (%)	Silt (%)	Clay (%)	Tidal channel pattern	Altitude/Slope
A	A24	Mud flat gM (gravelly Mud)	6.58	45.06	23.54	complex and meandering with oyster reefs	Lower part /steep
	H27	Mud flat sM (sandy Mud)	14.42	46.16	39.42	complex and meandering with oyster reefs	Upper part /steep
	H28	Mud flat sZ (sandy Silt)	26.15	49.76	24.09	complex and meandering with oyster reefs	Upper part /steep
	H40	Mud flat M (Mud)	15.9	49.33	34.77	complex and meandering	Upper part /steep
B	A18	Mixed flat mS (muddy Sand)	62.59	22.67	14.74	simple and straight	Middle part /gentle
	H32	Mixed flat zS (silty Sand)	54.87	31.36	13.77	simple and straight	Middle part /gentle
	H57	Mixed flat mS (muddy Sand)	78.59	11.54	9.87	simple and straight	Middle part /gentle
	OC14	Sand flat gS (gravelly Sand)	75.73	0.15	0.30	not present	Upper part /steep
C	H25-1	Sand flat msG (muddy sandy gravel)	61.39	2.89	5.02	simple and straight	Upper part /steep
	H64	Sand flat (g)S (slightly gravelly Sand)	89.82	4.58	5.26	not present	Lower part /gentle
D	H23-1	Sand flat gmS (gravelly muddy Sand)	57.24	14.49	13.96	simple and straight with shell framents	Lower part /gentle

In a study by Kim *et al.* [45], red, green, and blue (RGB) orthoimagery from an unmanned aerial vehicle was used in combination with a field survey (232 samples) to produce a large-scale classification map for surface-sediment distribution, in accordance with sedimentology standards. The object-based method employed in that study was used to classify surface-sediment distribution based on correlations with spectral reflectance, grain size, and tidal channels. Six sediment types were distinguished according to their spectral reflectance and sediment properties, such as grain composition, and statistical parameters. In the present study, the classification was based on the four groups of Folk and Ward [27], and the mapping results were similar to the four statistically processed groups.

A comparative evaluation of this study with previous studies showed that the seawater circulation in the northern part of Cheonsu Bay was changed by the embankment, thus affecting the sediment circulation. Changes in sedimentary patterns, rather than in the exposure time, accounted for the differences in the sediment compositions of the upper, middle, and lower stations, a response that is expected to continue. High organic carbons or benthic organisms will likewise be affected.

Minimizing the impact on the ecosystem of the Hwangdo tidal flats in Cheonsu Bay caused by these changes, and preservation of the tidal flats and surrounding waters, will require implementation of a management plan for the sedimentary environment, one that takes into account the survey results of continuous monitoring. In future studies, a dataset comprising geological environment characteristics, obtained based on the approach used in this study, will be used to assess changes in tidal-flat topography and the sedimentation environment. The results will contribute to improved management and conservation of tidal flats.

Author Contributions: Conceptualization, J.-h.L. and H.J.W.; methodology, J.-h.L.; validation, J.-h.L, H.J.W. and H.-s.J.; formal analysis, J.-h.L, H.J.W. and H.-s.J.; investigation, J.-h.L, Y,J., J.B.J., J.H.S. and K.K.; data curation, J.-h.L.. Y. J., J.H.S. and K.K.; writing— original draft preparation, J.-h.L.; writing—review and editing, J.-h.L., H.J.W.. and H.-s.J.; visualization, J.-h.L. and Y.J.; supervision, J.-h.L., H.J.W. and J.-h.R.; project administration, J.-h.L., K. K. and J.-h.R.; funding acquisition, J.-h.R. All authors have read and agreed to the published version of the manuscript.

Funding: This study was supported by the "Development of technology for constructing biological and environmental spatial information system of tidal flats through machine learning of remotely sensed visual data (2023, PEA0115)" funded by Korea Institute of Ocean Science & Technology (KIOST) and a project titled "Development of change monitoring technique for Tidal flat Spatial Information (TSI)" funded by the Korea Institute of Marine Science & Technology (2023, PM63870, Ministry of Oceans and Fisheries, South of Korea).

Institutional Review Board Statement: Not applicable.

Informed Consent Statement: Not applicable.

Data Availability Statement: The dataset supporting this study's findings and tables are deposited in Korea Institute of Ocean Science & Technology (KIOST). It is stored in the research cloud. If you need a dataset, please contact the corresponding author by e-mail (leejh@kiost.ac.kr) and we will reply within 14 days.

Conflicts of Interest: The authors declare no conflict of interest.

References

1. Woo, H.J.; Choi, J.U.; Ryu, J.H.; Choi, S.H.; Kim, S.R. Sedimentary environments in the Hwangdo tidal flat, Cheonsu Bay. *Korean Journal of Wetlands Research*. **2005**, *7*, 53-67.
2. Zheng, Q.A.; Klemas, V. Determination of winter temperature patterns, fronts, and surface currents in the Yellow Sea and East China Sea from satellite imagery. *Remote Sens. Environ.* **1982**, *12*, 201-218.
3. Lee, H.J.; Chough, S.K. Sediment distribution, dispersal and budget in the Yellow Sea. *Mar. Geol.* **1980**, *87*, 195-205.
4. Oh, J.K.; Han, C.H. Depositional environment of sandy tidal flat in Anmyeondo, Western Coast of Korea. *Journal of the Korean earth science society*. **2010**, *31*, 139-150.
5. Lee, H.B.; Kim, S.U. Sedimentologic and mineralogic study in surface sediment off Biin Bay, west coast of Korea. *Journal of the Korean earth science society*. **1997**, *18*, 259-259.
6. Ryu, S.O.; Chang, J.H. Characteristics of tidal beach and shoreline changes in Chonsu Bay, west coast of Korea. *Journal of the Korean earth science society*. **2005**, *26*, 584-596.
7. Woo, H.J.; Choi, J.U.; An, S.; Kwon, S.J.; Koo, B.J. Changes of sedimentary environments in the Saemangeum tidal flat on the west coast of Korea. *Korean Ocean Polar Res.* **2006**, *26*, 361-368.
8. Chang, J.H.; Ryu, S.O; Jo, Y.J. Long-term variation of tidal-flat sediments in Gomso Bay, west coast of Korea. *Journal of the Korean earth science society*. **2007**, *28*, 357-366.
9. Oh, J.K.; Choi, K.HJ. Environment of deposition and characters of surface sediments in the nearshore off Byun-San Peninsula, Korea. *The Sea: Journal of the Korean Society of Oceanography.* **1999**, *4*, 107-116.
10. Oh, J.K.; Kum, B.C. Depositional environments and characteristics of surface sediments in the nearshore and offshore off the mid-western coast of the Korean Peninsula. *Journal of the Korean earth science society.* **2007**, *22*, 377-387.
11. Ryu, S.O. Seasonal variation patterns of tidal flat sediments in semi-enclosed Hampyong and Kwangyang Bays, west and south coasts of Korea. *Journal of the Korean earth science society.* **2003**, *24*, 578-591.
12. Woo, H.J. Long-term changes of sediment and topography at the southern Kanghwa tidal flat, west coast of Korea. *Korean Journal of Wetlands Research*. **2013**, *22*, 493-500.

13. Choi, Y.S.; Song, J.H.; Yoon, S.P.; Chung, S.O. The environmental characteristics and factors on the cultured manila clam (*Ruditapes philippinarum*) at Hwangdo and Jeongsanpo of Taean in the west coast of Korea. *The Korean Journal of Malacology*. **2014**, *30*, 117-126.

14. So, J.G.; Jeong, G.T.; Chae, J.W. Numerical modeling of changes in tides and tidal currents caused by embankment at Chonsu Bay. *Journal of Korean Society of Coastal and Ocean Engineers*. **1998**, *10*, 151-164.

15. Shim, J.H.; Lee, W.H.; Chae, J.W. On phytoplankton of the Cheonsu Bay, West Coast. *The Sea: Journal of the Korean Society of Oceanography*. **1979**, *14*, 6-14.

16. Shim, J.H.; Yun, K.H. Seasonal variation and production of zooplankton in Chosu Bay, Korea. *The Sea: Journal of the Korean Society of Oceanography*. **1990**, *25*, 229-239.

17. Park, H.S.; Lim, H.S.; Hong, J.S. Spatio and temporal patterns of benthic environment and macrobenthos community on subtidal soft bottom in Chonsu Bay, Korea. *The Korean Society of Fish. Aquatic Sci.* **2000**, *33*, 262-271.

18. Kim, G.H. A Study on the sedimentation effect in Cheonsu Bay. Master's Thesis, *Korean Seoul National University*. **1979**, 1-28.

19. Kim, S.G. A study on the organization of sediments in the intertidal zone of the coast of Hongseong-gun in Cheonsu Bay, Master's Thesis, *Korean Gongju Normal University*. **1987**, p. 63.

20. Kim, Y.S. The Sedimentology of holocene intertidal deposits in Cheonsu Bay, West Coast of Korea. *The Korean Earth Science Society.* **1989**, *10*, 134-134.

21. Kim, Y.S.; Kim, J.N. Biogenic sedimentary structures of crustaceans at the intertidal flat of Whang Island, Cheonsu Bay. *The Korean Earth Science Society.* **1996**, *17*, 357-364.

22. Kim, J.H. A study on the distribution of sediments in the northern part of Cheonsu Bay in the West Sea of Korea, Master's Thesis, *Korean Gongju Normal University*. **2000**, p. 42.

23. Choi, J.K.; Ryu, J.H. A study on the sedimentary facies change in the tidal flat using high spatial resolution remotely sensed data. *Econ. Environ. Geol.* **2011**, 44, 59-70.

24. Kim, Y.S. The sedimentology of Holocene intertidal deposits in Cheonsu Bay, west coast of Korea. *Journal of Korean Earth Science Society*. **1989**, 10, 134-151.

25. Yoon, J.J. Evaluation of the tidal-flat ecosystem restoration effect on the construction of Hwangdo Bridge in Taean. *Korean Journal of Coastal Disaster Prevention*. **2021**, 8, 79-88.

26. Folk, R.L. Petrology of sedimentary rocks, Hemphill's, **1968**, p. 170.

27. Folk, R.L.; Ward, W. Brazos river bar: A study in the significance of grain size parameters. *J. Sediment. Res.* **1957**, 27, 3-26.

28. Lee, J.H.; Park, K.S.; Woo, H.J. Characteristics of total carbon and total organic carbon using elemental analyzer in Hyung-do intertidal zone sediments. *Korean Econ. Environ. Geol.* **2012**, 45, 673-684.

29. Lee, J.H.; Jeong, K.S.; Lee, D.H.; Park, K.S.; Woo, H.J. Elemental (C/N Ratios) Isotope compositions ($\delta^{13}C_{TOC}$ and $\delta^{15}N_{TN}$) of surface sediments from the barrier islands in the Nakdong river estuary, South Korea. *J. Coast. Res. Special Issue (SI)*. **2018**, 85, 36-40.

30. Ryu, J.H.; Na, Y.H.; Won, J.S.; Doerffer, R. A critical grain size for Landsat ETM+ investigations into intertidal sediments: a case study of the Gomso tidal flats, Korea. *Estuar. Coast. Shelf Sci.* **2004**, 60, 491-502.

31. Rainey, M.P.; Tyler, A.N.; Bryant, R.G.; Gilvear, D.J.; McDonald, P. The influence of surface and interstitial moisture on the spectral characteristics of intertidal sediments: implications for airborne image acquisition and processing. *Int. J. Remote Sens.* **2000**, 21, 3025-3038.

32. Brady, N.C.; Weil, R.R.; Weil, R.R. The nature and properties of soils. *Upper saddle river, NJ: Prentice Hall*, **2008**, 13, 662-710.

33. Avnimelech, Y.; Ritvo, G.; Meijer, L.E.; Kochba, M. Water content, organic carbon and dry bulk density in flooded sediments. *Aquac. Eng.* **2001**, 25, 25-33.

34. Danielson, R.E.; Sutherland, P.L. Porosity. In: Klute, A. (eds), Methods of soil analysis, Part 1, Physical and mineralogical methods, *Am. Soc. Agr., Inc.*, Madison, Wisconsin, **1986**. 443–461.

35. Olkin, I.; Sampson, A.R. Multivariate analysis: Overview in Smelser, Neil J.; Baltes, Paul B. (eds.), *International encyclopedia of the social & behavioral sciences, Pergamon,* ISBN 9780080430768, retrieved 2019-09-02, **2001**, pp. 10240–10247.

36. Ryu, J.H.; Cho, W.J.; Won, J.S.; Lee, I.T.; Chun, S.S.; Suh, A.S.; Kim, K.L. Intertidal DEM generation using waterline extracted from remotely sensed data. *Korean J. Remote. Sens.* **2000**, 16, 221-233.

37. Bartholdy, J.; Folving, S. Sediment classification and surface type mapping in the Danish Wadden Sea by remote sensing. *Neth. j. sea res.* **1986**, 20, 337-345.

38.   Yates, M.G.; Jones, A.R.; McGrorty, S.; Goss-Custard, J.D. The use of satellite imagery to determine the distribution of intertidal surface sediments of the Wash, England. *Estuar. Coast. Shelf Sci.* **1993**, 36, 333-344.

39.   Rainey, M.P.; Tyler, A.N.; Gilvear, D.J.; Bryant, R.G.; McDonald, P. Mapping intertidal estuarine sediment grain size distributions through airborne remote sensing. *Remote Sens. Environ.* **2003**, 86, 480-490.

40.   Ryu, J.H.; Ahn, Y.H.; Woo, H.J., Park; C.H.; Yoo, H.R.; Won, J.S. Qualitative classification of the surface sedimentary facies of tidal flat using high resolution satellite data - A case study of Hwangdo tidal flat in Cheonsu Bay. *Journal of the Geological Society of Korea*, **2005**, 41,199-210.

41.   Kim, K.L.; Ryu, J.H. Mapping oyster reef distribution using Kompsat-2/3 and linear spectral unmixing algorithm - A case study at Hwangdo tidal flat. *J. Coast. Res. Special Issue (SI)*. **2020**. 102, 246-253.

42.   Eom, J.; Choi, J.K.; Lee, Y.K.; Ryu, J.H.; Won, J.S. Standardization of sedimentary facies and topography based on the tidal channel type in Western coastal area, Korea. *J. Coast. Res.* **2013**, 65. 1373-1378.

43.   Kim, K.; Jung, H.C.; Choi, J.K.; Ryu, J.H. Statistical Analysis for tidal flat classification and topography using multitemporal SAR backscattering coefficients. *Remote Sens.* **2021**, 13, 5169.

44.   Kim, K.L.; Choi, J.K.; Ryu, J.H. The dataset of sedimentary environments at Hwangdo tidal flat on the western coast of Korea (2004 to 2013). *Korean Data of Geology, Ecology, Oceanography, Space Science, Polar Science,* **2020**. 2, 33-44.

45.   Kim, K.L.; Kim, B.J.; Lee, Y.K.; Ryu, J.H. Generation of a large-scale surface sediment classification map using unmanned aerial vehicle (UAV) data: A case study at the Hwang-do tidal flat, Korea. *Remote Sens.* **2019**. 11, p.229.